Journal of Applied Fluid Mechanics , Vol. 9, No. 2, pp. 945-955, 2016.
Available online at www.jafmonline.net, ISSN 1735-3572, EISSN 1735-3645.
DOI: 10.18869/acadpub.jafm.68.225.24053

Conjugate Natural Convection Heat Transfer in a Rotating Enclosure

H. Saleh[1†] and I. Hashim[1,2,3]

[1] *School of Mathematical Sciences, Universiti Kebangsaan Malaysia, 43600 UKM Bangi Selangor, Malaysia*
[2] *Solar Energy Research Institute, Universiti Kebangsaan Malaysia, 43600 UKM Bangi Selangor, Malaysia*
[3] *Research Institute Center for Modeling & Computer Simulation (RI/CM&CS), King Fahd University of Petroleum & Minerals, Dhahran-31261, Saudi Arabia*

† *Corresponding Author Email*: *Dr.habibissaleh@gmail.com*

(Received September 12, 2014; accepted January 7, 2015)

ABSTRACT

The aim of the present numerical study to analyze the conjugate natural convection heat transfer in a rotating enclosure with finite wall thickness. The enclosure executes a steady counterclockwise angular velocity about its longitudinal axis. The staggered grid arrangement together with the Marker and Cell (MAC) method was employed to solve the governing equations. The governing parameters considered are the wall thickness, $0.05 \leq D \leq 0.2$, the conductivity ratio, $0.5 \leq Kr \leq 10$ and the Taylor number, $8.9 \times 10^4 \leq Ta \leq 1.1 \times 10^6$, and the centrifugal force is assumed weaker than the Coriolis force. It is found that decreasing the conductivity ratio or/and rotational speed stabilize of the convective flow and heat transfer oscillation. The global quantity of the heat transfer rate increases by increasing the conductivity ratio and it decreases about 12% by increasing 20% wall thickness for the considered rotational speeds.

Keywords: Finite difference method; Conjugate heat transfer; Rotating enclosure.

NOMENCLATURE

Cp	specific heat capacity (J/kg K)
g	gravitational acceleration (m/s^2)
k	thermal conductivity (W m^{-1} K^{-1})
ℓ	width and height of enclosure (m)
Nu	Nusselt number
p	pressure (N/m^2)
Pr	Prandtl number
Ra	Rayleigh number
Ra_ω	rotational Rayleigh number
t	time (s)
Ta	Taylor number
T	temperature (K)
u, v	velocity components (m/s)
x, y	space coordinates (m)
α	thermal diffusivity (m^2/s)
β	thermal expansion coefficient (1/K)
ν	kinematic viscosity (m^2/s)
τ	dimensionless time
τ_p	dimensionless time for one rotation
Θ	dimensionless temperature
Ω	angular rotation rate (rpm,rad/s)
ρ	density (kg/m^3)
φ	angular position(rad)
μ	dynamic viscosity (N s/m^2)

1. INTRODUCTION

Natural convection in enclosures is a challenging topic of practical importance, because enclosures filled with fluid are central components in a long list of engineering and geophysical systems as well as academic researches. The conductivities of the material of the thermal systems is very important in many situations, for example, in a high performance insulation for buildings. This coupled conduction-convection problem is known as conjugate convection. Conjugate natural convection in a rectangular enclosure surrounded by walls was firstly examined by Kim and Viskanta (1984), Kim and Viskanta (1985). Their results show that wall conduction effects reduce the average temperature differences across the cavity, par-

tially stabilize the flow and decrease the heat transfer rate. Kaminski and Prakash (1986) and Misra and Sarkar (1997) performed a numerical study on conjugate convection in a square enclosure with thick conducting wall on one of its vertical sides. The influence of wall conduction on natural convection in an inclined square enclosure was examined by Acharya and Tsang (1987), Yedder and Bilgen (1997) and Nouanegue, Muftuoglu, and Bilgen (2009). Du and Bilgen (1992) found that the temperature distribution on the solid–fluid interface is greatly influenced by the coupling effect between solid wall conduction and fluid convection. Mobedi (2008) focused on the horizontal conductive walls of conjugate convection in cavities and he showed that the heat transfer rate is also affected by the combination of Rayleigh number and the thermal conductivity ratio. Recently, Zhang, Zhang, and Xi (2011) studied conjugate heat transfer in a tilted enclosure with time-periodic sidewall temperature. They found that the heat transfer rate increases almost linearly with the thermal conductivity ratio and the thermal diffusivity ratio due to wall conduction.

Natural convection in a rotating rectangular box has been numerically studied by Buhler and Oertel (1982). They found the roll cells changed orientation with increasing the rotation speeds. Hamady, Lloyd, Yang, and Yang (1994) investigated numerically and experimentally fluid flow and heat transfer characteristics of a rotating square enclosure. They concluded that the Coriolis force arising from rotation may have a remarkable influence on heat transfer when compared with non-rotating results and a correlation of Nusselt number as function of Taylor and Rayleigh number were built. Lee and Lin (1996) and Ker and Lin (1996), Ker and Lin (1997) studied a differentially heated rotating cubic enclosure. Significant flow modification was obtained when the rotational Rayleigh number greater than the Rayleigh number or the Taylor number greater than the Rayleigh number and examined effect of the rotation to the flow stabilization. A significant increasing or decreasing in heat transfer in a rotating and differentially heated square enclosure could be achieved due to rotational effects as reported by Baig and Masood (2001) and Baig and Zunaid (2006). Jin, Tou, and Tso (2005) studied numerically the rectangular enclosure with discrete heat sources and found rotation results in imbalance of clockwise and counterclockwise circulations, increases heat transfer in the worst stage, reduces the oscillation of Nusselt number, and improves or reduces mean performance in each cycle. The effects of Coriolis force, centrifugal force, and thermal buoyancy force were segregated numerically by Tso, Jin, and Tou (2007) on a differentially heated square enclosure. The effects of the Coriolis and centrifugal forces were found small and differentiated from those other forces. Mukunda, Shailesh, Kiran, and Shrikantha (2009) studied the behaviour of the fluids rotating from zero to critical speed.

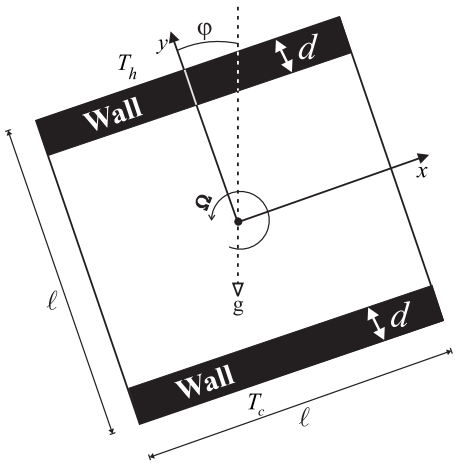

Fig. 1. Schematic representation of the model.

Best of authors knowledge, the study on conjugate convection in rotating enclosures with wall conduction effect is not studied so far. So, the problem of conjugate convection heat transfer in a rotating enclosure is studied numerically in the present study. The effects of wall thickness and conductivity ratio wall to fluid as well as the rotational speeds on characteristics of convective flow and heat transfer performance are considered.

2. MATHEMATICAL FORMULATION

A schematic diagram of a square enclosure with finite wall thickness d of side ℓ executes a steady uniform counterclockwise angular velocity about its longitudinal as shown in Fig. 1., with the geometric layout and the Cartesan coordinates (x,y) rotating with the enclosure. The surface at $y = \ell/2$ has constant hot temperature (T_h) and the surface at $y = -\ell/2$ has a constant cold temperature (T_c). The temperatures along the lateral wall are assumed to be linearly distributed between T_h and T_c, i.e. $(T_h+T_c)/2+(T_h-T_c)y/\ell$ to consider conjugate heat transfer in the lateral wall of the experiments. The φ shown in the Fig. 1. is defined as an angular position.

The fluid is Newtonian and the flow is laminar and incompressible. The density variation of the fluid follows Boussinesq's assumption and changes with temperature only. The terms representing the thermal and rotational buoyancies and Coriolis force are, respectively, equal to $\rho_0 \mathbf{g}\beta(T_f - T_c)$, $-\rho_0 \mathbf{g}\beta(T_f - T_c)\Omega \times (\Omega \times \mathbf{r})$, and $-2\rho_0[1-\beta(T_f - T_c)] \cdot \Omega \times \mathbf{V}$. The continuity, momentum and energy equations can be described as follows:

$$\frac{\partial u}{\partial x} + \frac{\partial v}{\partial y} = 0 \tag{1}$$

$$\frac{\partial u}{\partial t} + u\frac{\partial u}{\partial x} + v\frac{\partial u}{\partial y} = -\frac{1}{\rho_0}\frac{\partial P_m}{\partial x}$$

$$+\nu\left(\frac{\partial^2 u}{\partial x^2} + \frac{\partial^2 u}{\partial y^2}\right) + 2\Omega v - 2\Omega v\beta(T_f - T_c)$$

$$-\Omega^2 x\beta(T_f - T_c) + g\beta(T_f - T_c)\sin(\Omega t) \tag{2}$$

$$\frac{\partial v}{\partial t} + u\frac{\partial v}{\partial x} + v\frac{\partial v}{\partial y} = -\frac{1}{\rho_0}\frac{\partial P_m}{\partial y}$$

$$+\nu\left(\frac{\partial^2 v}{\partial x^2} + \frac{\partial^2 v}{\partial y^2}\right) - 2\Omega u + 2\Omega u\beta(T_f - T_c)$$

$$-\Omega^2 y\beta(T_f - T_c) + g\beta(T_f - T_c)\cos(\Omega t) \tag{3}$$

$$\frac{\partial T_f}{\partial t} + u\frac{\partial T_f}{\partial x} + v\frac{\partial T_f}{\partial y} = \alpha\left(\frac{\partial^2 T_f}{\partial x^2} + \frac{\partial^2 T_f}{\partial y^2}\right) \tag{4}$$

and the energy equation for the impermeable wall is:

$$\frac{\partial^2 T_w}{\partial x^2} + \frac{\partial^2 T_w}{\partial y^2} = 0 \tag{5}$$

where P_m is the motion pressure defined as:

$$\begin{aligned} P_m &= p - \frac{1}{2}\rho_0\Omega^2 x^2 - \frac{1}{2}\rho_0\Omega^2 y^2 \\ &\quad + \rho_0 g x\sin(\Omega t) + \rho_0 g y\cos(\Omega t) \end{aligned} \tag{6}$$

Hence,

$$-\frac{\partial P_m}{\partial x} = -\frac{\partial p}{\partial x} + \rho_0\Omega^2 x - \rho_0 g\sin(\Omega t) \tag{7}$$

$$-\frac{\partial P_m}{\partial y} = -\frac{\partial p}{\partial y} + \rho_0\Omega^2 y - \rho_0 g\cos(\Omega t) \tag{8}$$

The governing equations (2)–(4) can be converted to nondimensional forms using the following nondimensional parameters:

$$X = \frac{x}{\ell}, Y = \frac{y}{\ell}, \tau = \frac{t\alpha}{\ell^2}, U = \frac{u\ell}{\alpha}, V = \frac{v\ell}{\alpha},$$

$$\Theta_f = \frac{T_f - T_c}{T_h - T_c}, Pr = \frac{\nu}{\alpha}, Ra = \frac{g\beta(T_h - T_c)\ell^3}{\nu\alpha},$$

$$P = \frac{P_m\ell^2}{\rho\alpha^2}, \quad \Theta_w = \frac{T_w - T_c}{T_h - T_c}, D = \frac{d}{\ell} \tag{9}$$

$$Ra_\omega = \frac{\beta\Omega^2(T_h - T_c)\ell^4}{\nu\alpha}, Ta = \frac{4\Omega^2\ell^4}{\nu^2}$$

The Coriolis buoyancy force is neglected, because $|\beta(T - T_c)| << 1$ in the present studies. The nondimensional continuity, momentum, and energy equations are written as follows:

$$\frac{\partial U}{\partial X} + \frac{\partial V}{\partial Y} = 0 \tag{10}$$

$$\frac{\partial U}{\partial \tau} + U\frac{\partial U}{\partial X} + V\frac{\partial U}{\partial Y} = -\frac{\partial P}{\partial X}$$

$$+Pr\left(\frac{\partial^2 U}{\partial X^2} + \frac{\partial^2 U}{\partial Y^2}\right) + \underbrace{Ta^{0.5}PrV}_{\text{Coriolis force term}}$$

$$-\underbrace{Ra_\omega PrX\Theta_f}_{\text{Centrifugal force term}} + \underbrace{RaPr\Theta_f\sin(0.5Ta^{0.5}Pr\tau)}_{\text{Buoyancy force term}} \tag{11}$$

$$\frac{\partial V}{\partial \tau} + U\frac{\partial U}{\partial X} + V\frac{\partial U}{\partial Y} = -\frac{\partial P}{\partial X}$$

$$+Pr\left(\frac{\partial^2 U}{\partial X^2} + \frac{\partial^2 U}{\partial Y^2}\right) - \underbrace{Ta^{0.5}PrU}_{\text{Coriolis force term}}$$

$$-\underbrace{Ra_\omega PrY\Theta_f}_{\text{Centrifugal force term}} + \underbrace{RaPr\Theta_f\cos(0.5Ta^{0.5}Pr\tau)}_{\text{Buoyancy force term}} \tag{12}$$

$$\frac{\partial \Theta_f}{\partial \tau} + U\frac{\partial \Theta_f}{\partial X} + V\frac{\partial \Theta_f}{\partial Y} = \frac{\partial^2 \Theta_f}{\partial X^2} + \frac{\partial^2 \Theta_f}{\partial Y^2} \tag{13}$$

$$\frac{\partial^2 \Theta_w}{\partial X^2} + \frac{\partial^2 \Theta_w}{\partial Y^2} = 0 \tag{14}$$

$U = V = 0$ on the walls and the boundary conditions for the non-dimensional temperatures are:

$$\Theta_w = Y + 0.5 \text{ and } \Theta_f = Y + 0.5 \text{ at } X = -0.5, X = 0.5 \tag{15}$$

$$\Theta_w = \Theta_f \text{ and } \frac{\Theta_f}{\partial Y} = Kr\frac{\partial \Theta_w}{\partial Y} \text{ at } X = D, X = 1 - D \tag{16}$$

$$\Theta_w = 0 \text{ at } Y = -0.5 \text{ and } \Theta_w = 1 \text{ at } Y = 0.5 \tag{17}$$

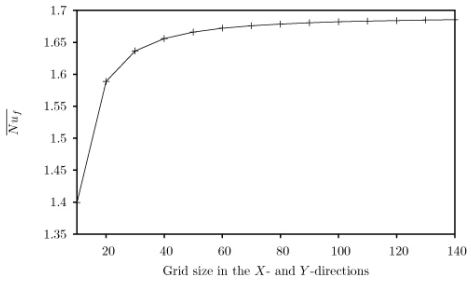

(a)

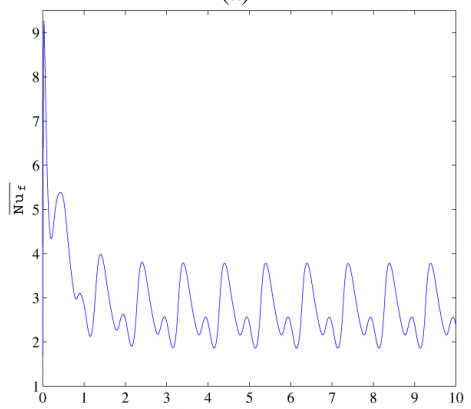

(b)

Fig. 2. (a) Grid independency study: $\overline{Nu_f}$ versus number of grid points, (b) Typical computation process for present periodic oscillation problem.

where $Kr = k_w/k_f$ is the thermal conductivity ratio.

The fluid motion is displayed using the stream function Ψ obtained from velocity components U and V. The relationships between the stream function and the velocity components are: $U = \partial\Psi/\partial Y$ and $V = -\partial\Psi/\partial X$, which yield a single equation,

$$\frac{\partial^2\Psi}{\partial X^2} + \frac{\partial^2\Psi}{\partial Y^2} = \frac{\partial U}{\partial Y} - \frac{\partial V}{\partial X} \tag{18}$$

where $\Psi = 0$ at all walls of the enclosure. The physical quantities of interest in this problem are the average Nusselt number, representation of the average heat transfer rate on the solid–fluid interface that defined by:

$$\overline{Nu_f} = \int_{-0.5}^{0.5} \frac{\partial\Theta_f}{\partial Y}\,\mathrm{d}X \tag{19}$$

The time-integrated of the average heat transfer rate in one cycle is:

$$\overline{\overline{Nu_f}} = \int_0^{\tau_p} \overline{Nu_f}\,\mathrm{d}\tau \tag{20}$$

3. NUMERICAL METHOD AND VALIDATION

Staggered grid arrangement together with the Marker and Cell (MAC) method by Harlow and Welch (1965) are adopted to solve the governing equations (10)–(14) subject to the boundary conditions (15)–(17). Due to lack of boundary conditions for pressure, the use of the staggered grid and MAC formulation provide an advantage. That is, one may locate the secondary grid along the boundaries of the domain where only specification of velocity boundary conditions is required but not of the pressure. The fictitious values of velocity outside the domain are obtained by extrapolation of the interior points as given by Hoffmann and Chiang (2000). A second-order central difference approximation is used for the space discretization and a first-order approximation is used for temporal derivative. The solution of the Poisson pressure equation is obtained by applying an iterative Gaussian-SOR method. The velocities are then computed by the projection method.

In this study, the convergence criterion for the Poisson equation is set as $\varepsilon = 10^{-5}$ and the time stepping is chosen, $\Delta\tau = \lambda(1/4)(\Delta X)^2 Pr$ to meet stability criteria where λ is the safety factor with the value between 0 and 1. Uniform grid distribution is used for the whole enclosure. The effect of grid resolution was examined in order to select the appropriate grid density as demonstrated in Fig. 2(a) for $Kr = 5$, $D = 0.15$, $Ta = 8.97 \times 10^4$, $Ra = 1.2 \times 10^5$ at $\varphi = 5\pi/4$. The results indicate that an 120×120 mesh can be used in the final computations. A typical computation process for the present periodic oscillation problem is shown in Fig. 2(b) where, the final periodic oscillation of the $\overline{Nu}$ is obtained after three rotations. Therefore, all computations in this work were carried out beyond three rotations. As a validation, Fig. 3.,

Table 1 The difference of isotherms contour level between present work with literature result for a special case, $D = 0$, $Pr = 0.7$, $Ra = 1.2 \times 10^5$, $Ta = 8.9 \times 10^4$ at some heated position

Contour level	$\varphi = 0$	$\varphi = \pi/2$	$\varphi = 3\pi/2$
1	0.32%	0.63%	0.16%
3	0.53%	0.53%	1.33%
5	0.32%	0.32%	0.32%
7	0.46%	0.46%	0.46%
9	0.36%	0.53%	0.92%
11	0.29%	0.29%	0.29%
13	0.12%	0.37%	0.86%
15	0.09%	0.21%	0.11%

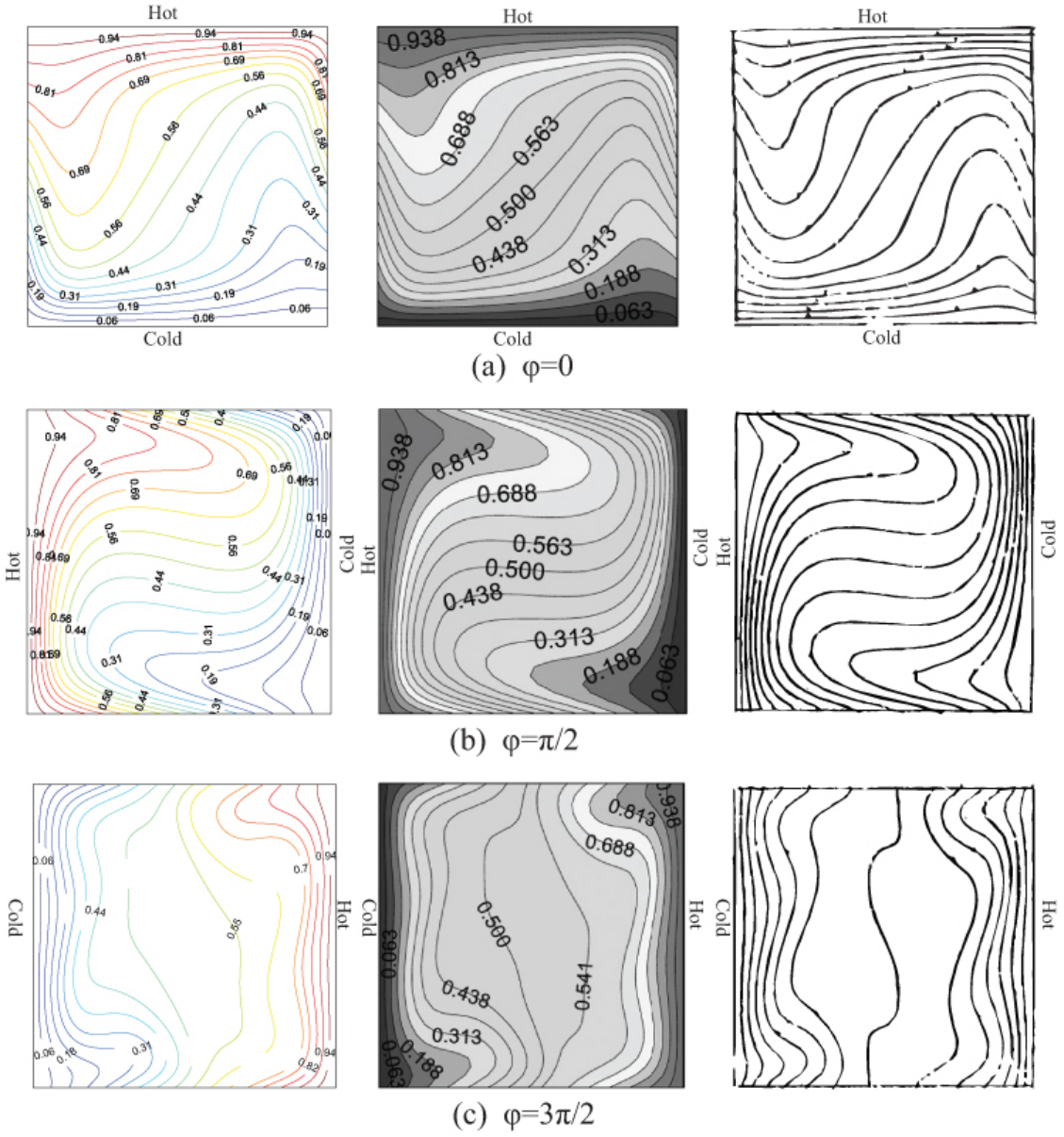

Fig. 3. Comparison of computed isotherms of present work with literature results for a special case, $D = 0$, $Pr = 0.7$, $Ra = 1.2 \times 10^5$, $Ta = 8.9 \times 10^4$.

our results (left) for the isotherms compare well with that obtained by Hamady, Lloyd, Yang, and Yang (1994) (middle) and Tso, Jin, and Tou (2007) (right) for a special case, $D = 0$, $Pr = 0.7$, $Ra = 1.2 \times 10^5$, $Ta = 8.9 \times 10^4$. In general, we observe less than 1% difference of the isotherms for various contour level at different φ as shown in Table. 1. The isotherm contour for level 3, $\varphi = 3\pi/2$ differs from that of Hamady, Lloyd, Yang, and Yang (1994) by about 1.33%. These differences may be attributed to the different method and meshes used by the Hamady, Lloyd, Yang, and Yang (1994).

Table 2 Fixed variables and constants

Parameter symbol	Magnitude
D	0.05 – 0.2
Kr	0.5 – 10
T_h	282 (K)
T_c	273 (K)
ℓ	0.0508 (m)
Pr	0.7
Ra	1.2×10^5
Ω	8.5 – 30.0 (rpm)
Ra_ω	496 – 2104
Ta	8.9×10^4–1.1×10^6

4. RESULTS AND DISCUSSION

The investigation in the undergoing numerical study is executed for the fixed variables and constants as tabulated in Table 2. The rotational Rayleigh number, Ra_ω, was not discussed except to specify it explicitly. This is due to the Ra_ω not being an independent parameter but depending on Pr and Ra as well as Ta. We note that in the present research the Coriolis force is stronger than the centrifugal force. The flow and temperature fields inside the enclosure during rotation will be shown in Fig. 4. and Fig. 5. The average Nusselt number over one period will be presented in Fig. 6. Finally, plots of the global quantity average Nusselt number over one cycle will be displayed in Fig. 7.

Fig. 4(a)-(h) shows the effects of rotation on the flow field for different thermal conductivities at $D = 0.15$ and $Ta = 8.9 \times 10^4$. There are two basic flow structures, clockwise (negative sign) and counterclockwise (positive sign) circulations, depending on the heated position as well as the inertial forces. Starting from $\varphi = \pi/4$ where the heated wall is above the cold wall, one observes a clockwise circulation induced by the buoyancy force. This flow circulation persists up to $\varphi = 5\pi/4$. At the $\varphi = 5\pi/4$, the gravitational force should reverses the flow direction when the the enclosure keep stationary, but the flow inertia from the previous circulation are superior compared to the buoyancy. At $\varphi = 3\pi/2$, Fig. 4(g), the effect of gravitational force now is to reverse the flow direction, but the flow inertia in the core still exist. The flows compete each other, where a clockwise cell in the core and two smaller cells in the corners rotating in a counterclockwise where the effect of the Coriolis force is small. With increasing angle the gravitational force increases so that the two vortex merge as shown in the Fig. 4(h). This is due to the Coriolis force directed from the center. It is interesting to note that the two swirling happen in the middle region for higher thermal conductivities but later these disappear by increasing the angle as depicted in Fig. 4(a) at $\varphi = 2\pi$ or 0 rad. These phenomena indicate lower thermal conductivities stabilize the fluid flow. Note that this sequence repeats itself, the fully clockwise cell then transition here as totally counterclockwise cell. It is observed that during rotation, the strength of the flow circulation of higher conductivities is always stronger than lower conductivities. Also, note that the flow patterns between $Kr = 1$ and $Kr = 0.5$ were different enough in some angular locations. The streamlines in all of the subplots (a)–(h) present centrosymmetry shape.

Fig. 5(a)-(h) exhibits the effects of rotation on the temperature field in the wall and fluid region for different thermal conductivity ratio at $D = 0.15$ and $Ta = 8.9 \times 10^4$. The heated wall positions move according to the angles of rotation. Starting from $\varphi = \pi/4$ where the heated wall above the cold wall. The solid wall temperature rise and followed by increasing the fluid adjoining the wall which creates a clockwise motion as shown in the previous figure. For larger Kr, more heat is transferred from the walls to the fluid that eventually intensified the natural convection. The isotherms are more distorted as the rotational angle takes higher up to $\varphi = \pi$, see Fig. 5(e). This is due to the Coriolis effect aids the main flow by the buoyancy force. Later, the isotherms distortion decrease by increasing the rotational angle. Later at $\varphi = 7\pi/4$, Fig. 5(h) and $\varphi = 2\pi$, Fig. 5(a), the isotherms of higher conductivities more distorted near the hot interface, but the isotherms of higher conductivities less distorted near the cold interface. It is also observed that almost straight lines were shown in the solid wall isotherm at any angular location. These phenomena indicate that conduction plays an important role in both solid walls.

Fig. 6(a),(b) and (c) depict the variation of the average Nusselt number, $\overline{Nu}_f$, over one period for different thermal conductivity ratio at

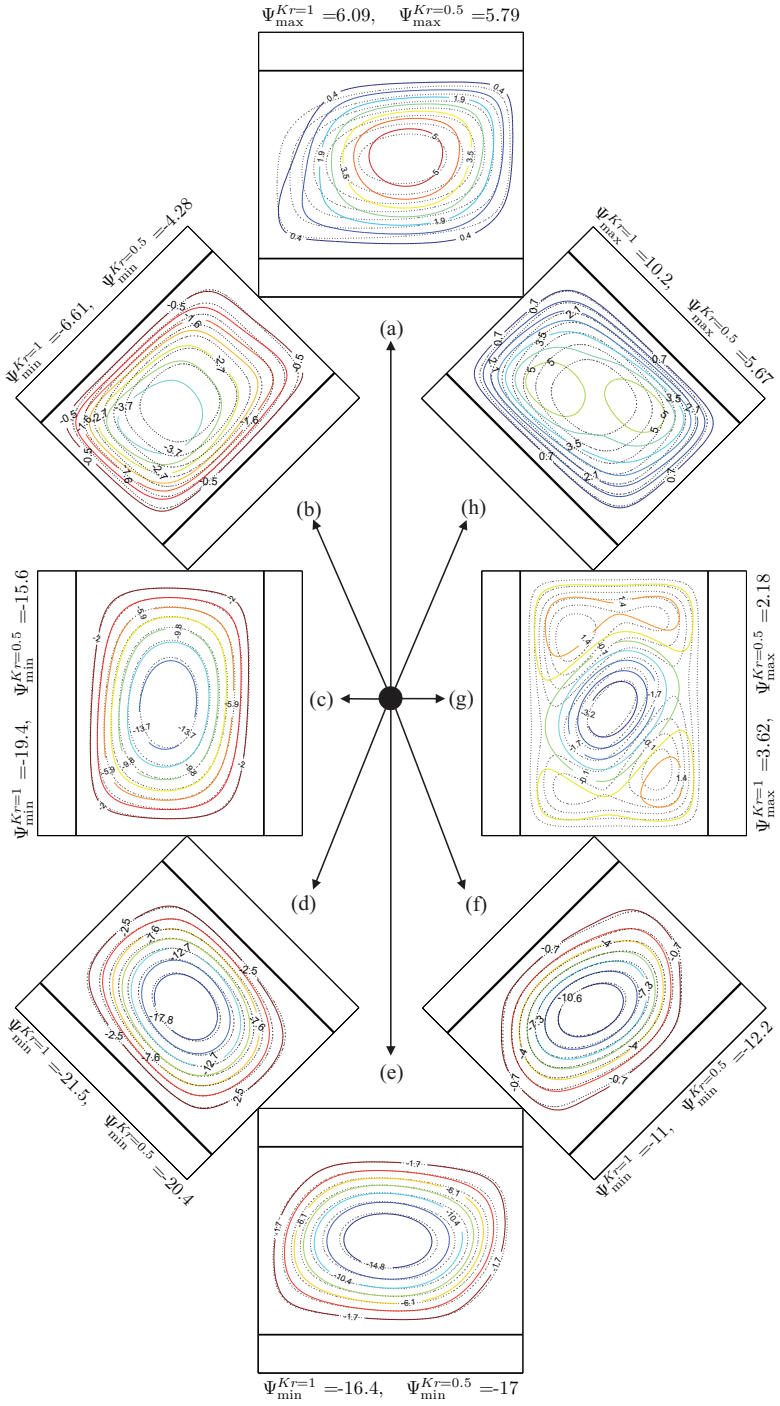

Fig. 4. Streamlines [$Kr = 1$ (solid lines) and $Kr = 0.5$ (dashed lines)] evolution during one period for $D = 0.15$ and $Ta = 8.9 \times 10^4$ when (a) $\varphi = 0$, (b) $\varphi = \pi/4$, (c) $\varphi = \pi/2$, (d) $\varphi = 3\pi/4$, (e) $\varphi = \pi$, (f) $\varphi = 5\pi/4$, (g) $\varphi = 3\pi/2$, (h) $\varphi = 7\pi/4$.

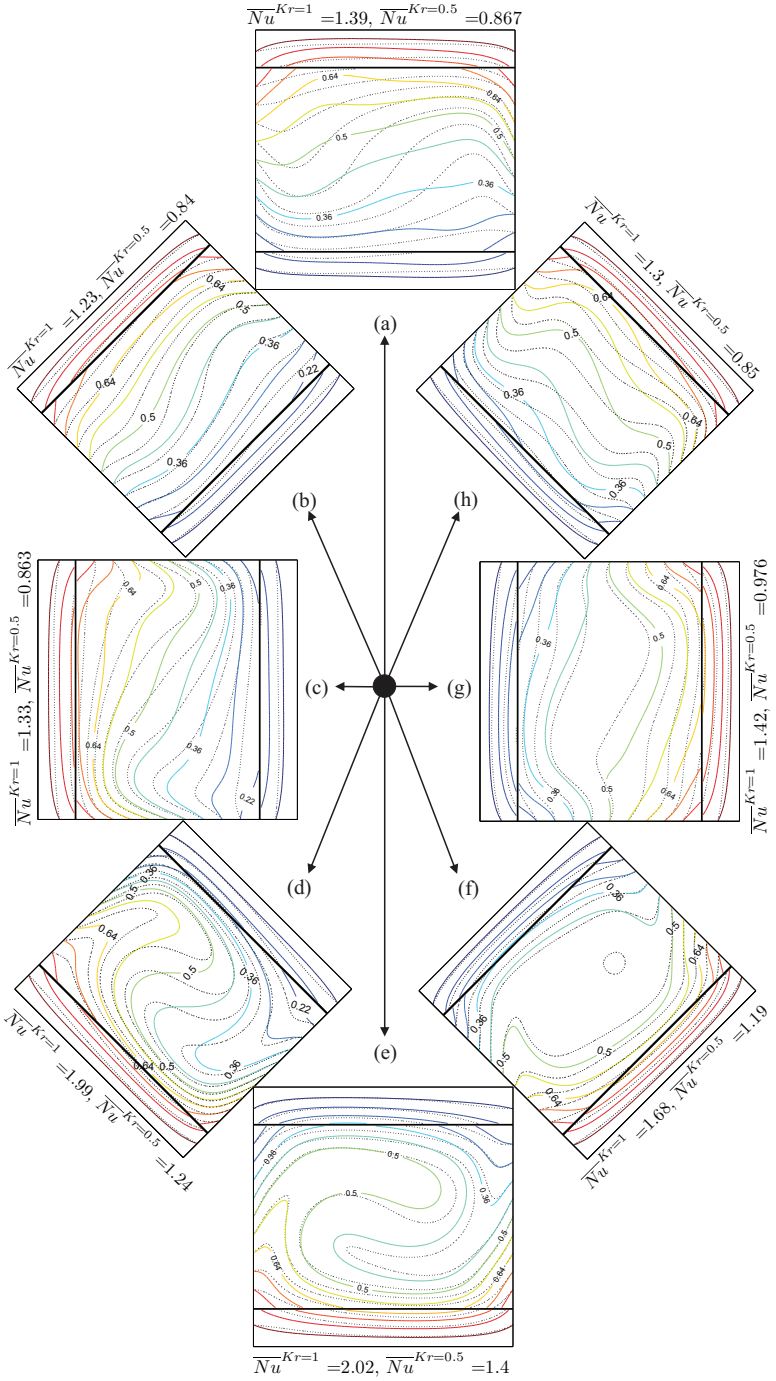

Fig. 5. Isotherms [$Kr = 1$ (solid lines) and $Kr = 0.5$ (dashed lines)] evolution during one period for $D = 0.15$ and $Ta = 8.9 \times 10^4$ when (a) $\varphi = 0$, (b) $\varphi = \pi/4$, (c) $\varphi = \pi/2$, (d) $\varphi = 3\pi/4$, (e) $\varphi = \pi$, (f) $\varphi = 5\pi/4$, (g) $\varphi = 3\pi/2$, (h) $\varphi = 7\pi/4$.

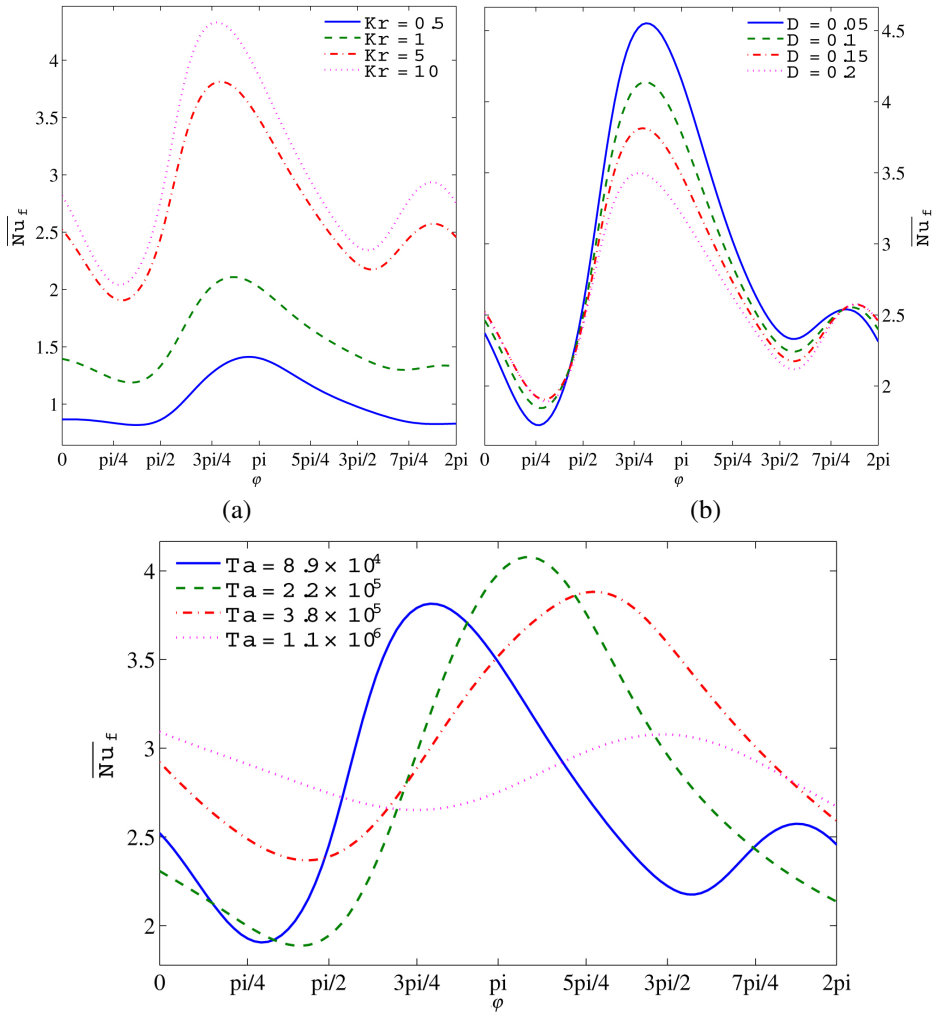

Fig. 6. Average Nusselt number against φ for the different values of *Kr* (a), *D* (b) and *Ta* (c).

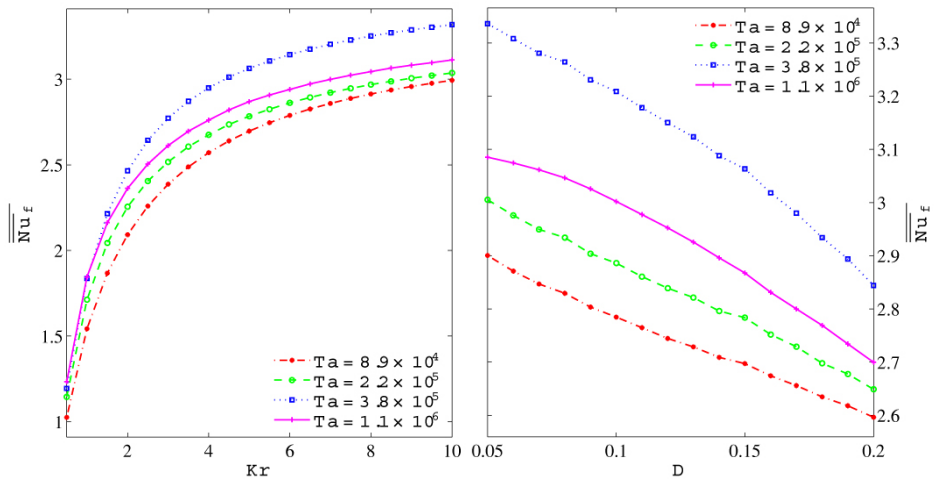

Fig. 7. Global quantity average Nusselt number for various values of *Ta* against, (a) *Kr* and (b) *D*.

$D = 0.15$, different wall thickness at $Kr = 5$ and $Ta = 8.9 \times 10^4$ and different rotational speeds (Taylor numbers) at $Kr = 5$ and $D = 0.15$, respectively. It observed that higher Kr lead to stronger $\overline{Nu}_f$ at any angular position as shown in Fig. 6(a). Decreasing the fluid conductivities can stabilize the heat transfer oscillating. It observed from Fig. 6(b) that thicker wall lead to stronger $\overline{Nu}_f$ at the peak. The average Nusselt number profiles display different characteristics for the various Taylor numbers as presented in Fig. 6(c). It observed that increasing the Taylor number stabilize the $\overline{Nu}$.

Fig. 7(a) and (b) show the the global quantity average Nusselt number for different Taylor numbers against the thermal conductivity ratio at $D = 0.15$ and against the wall thickness at $Kr = 5$, respectively. The global heat transfer performance increases nonlinearly by increasing the Kr as shown in Fig. 7(a). This is expected because convective wall provides more acquiescence to fluid flow. As a result of this phenomenon, for higher values of conductivity, isotherms are denser near the hot interface, which increases the temperature gradient in this region. It is also observed that at fixed Kr, higher rotational speeds lead to higher heat transfer rate, except at $Ta = 1.1 \times 10^6$ and $Kr > 1$ or when the fluid conductivity smaller than wall conductivity. The results demonstrated in Fig. 7(b) help to compare the heat transfer appearance by adjusting the wall thickness. The global heat transfer performance decreases about 12% by increasing 20% wall thickness for the considered rotational speeds. This result is consistent with the previous outcome where the solid wall becomes less and less conductive or behave as an insulated material. It is also observed that at fixed D, initially higher rotational speeds lead to higher $\overline{\overline{Nu}_f}$ but later the $\overline{\overline{Nu}_f}$ was dropped at maximum rotational speeds for the considered D interval.

5. CONCLUSIONS

Detailed computational results for flow fields and the conjugate heat transfer performance of the rotating enclosure with finite wall thickness have been presented in graphical forms. The periodic oscillation of the flow and temperature fields as well as the heat transfer were obtained. The main conclusions of the present analysis are as follows:

1. Decreasing the conductivity ratio or/and rotational speed stabilize of the convective flow and heat transfer oscillation.
2. The angular locations of the local maximum and minimum heat transfer are sensitive to the conductivity ratio, the wall thickness as well as the rotational speeds. The local maximum or minimum point tends to move to higher angle by expanding the wall thickness and it moves to lower angle when the conductivity ratio made higher.
3. The global quantity of the heat transfer rate increases by increasing the conductivity ratio and it decreases about 12% by increasing 20% wall thickness for the considered rotational speeds.

REFERENCES

Acharya, S. and C. H. Tsang (1987). Influence of wall conduction on natural convection in an inclined square enclosure. *Heat Mass Transf. 21*, 19–30.

Baig, M. and M. Zunaid (2006). Numerical simulation of liquid metals in differentially heated enclosure undergoing orthogonal rotation. *Int. J. Heat Mass Transf. 49*, 3500-3513.

Baig, M. F. and A. Masood (2001). Natural convection in a two-dimensional differentially heated square enclosure undergoing rotation. *Numer. Heat Transf. Part A 40*, 181–202.

Buhler, K. and H. Oertel (1982). Thermal cellular convection in rotating rectangular boxes. *J. Fluid Mech. 114*, 261-282.

Du, Z. G. and E. Bilgen (1992). Coupling of wall conduction with natural convection in a rectangular enclosure. *Int. J. Heat Mass Transf. 35*, 1969–1975.

Hamady, F. J., J. R. Lloyd, K. T. Yang and H. Q. Yang (1994). A study of natural convection in a rotating enclosure. *J. Heat Transf. 116*, 136-143.

Harlow, F. and J. Welch (1965). Numerical calculation of time-dependent viscous incompressible flow of fluid with a free surface. *Physics of Fluids 8*, 2182–2189.

Hoffmann, K. A. and S. T. Chiang (2000). *Computational Fluid Dynamics Volume I*. Kansas: Engineering Education System.

Jin, L. F., S. K. W. Tou and C. P. Tso (2005). Effects of rotation on natural convection cooling from three rows of heat sources in a rectangular cavity. *Int. J. Heat Mass Transf. 48*, 3982–3994.

Kaminski, D. A. and C. Prakash (1986). Conjugate natural convection in a square enclosure: effect of conduction in one of the vertical walls. *Int. J. Thermal Sci. 29*, 1979–1988.

Ker, Y. T. and T. F. Lin (1996). A combined numerical and experimental study of air convection in a differentially heated rotating cubic cavity. *Int. J. Heat Mass Transf. 39*, 3193–3210.

Ker, Y. T. and T. F. Lin (1997). Time-averaged and reverse transition in oscillatory air convection in a differentially heated rotating cubic cavity. *Int. J. Heat Mass Transf. 40*, 3335–3349.

Kim, D. M. and R. Viskanta (1984). Study of the effects of wall conductance on natural convection in differently oriented square cavities. *J. Fluid Mech. 144*, 153–176.

Kim, D. M. and R. Viskanta (1985). Effect of wall heat conduction on natural convection heat transfer in a square enclosure. *J. Heat Transf. 107*, 139–146.

Lee, T. L. and T. F. Lin (1996). Transient three-dimensional convection of air in a differentially heated rotating cubic cavity. *Int. J. Heat Mass Transf. 39*, 1243-1255.

Misra, D. and A. Sarkar (1997). Finite element analysis of conjugate natural convection in a square enclosure with a conducting vertical wall. *Computer Methods in Applied Mechanics and Engineering 141*, 205–219.

Mobedi, M. (2008). Conjugate natural convection in a square cavity with finite thickness horizontal walls. *Int. Comm. Heat Mass Transf. 35*, 503–513.

Mukunda, P., R. Shailesh, A. Kiran and S. Shrikantha (2009). Experimental study of unsteady thermal convection in heated rotating inclined cylinders. *Journal of Applied Fluid Mechanics 2*, 39–43.

Nouanegue, H., A. Muftuoglu and E. Bilgen (2009). Heat transfer by natural convection, conduction and radiation in an inclined square enclosure bounded with a solid wall. *Int. J. Thermal Sci. 48*, 871–880.

Tso, C. P., L. F. Jin and S. K. W. Tou (2007). Numerical segregation of the effects of body forces in a rotating, differentially heated enclosure. *Numer. Heat Transf. Part A 51*, 85-107.

Yedder, R. B. and E. Bilgen (1997). Laminar natural convection in inclined enclosures bounded by a solid wall. *Heat Mass Transf. 32*, 455–462.

Zhang, W., C. Zhang and G. Xi (2011). Conjugate conduction-natural convection in an enclosure with time-periodic sidewall temperature and inclination. *Int. J. Heat Fluid Flow 32*, 52-64.